2000

Nonlinear Self-Organization in Photorefractive Materials

Partha P. Banerjee
University of Dayton, pbanerjee1@udayton.edu

Nickolai Kukhtarev
Alabama A & M University

John O. Dimmock
University of Alabama, Huntsville

Chapter 3

Nonlinear Self-Organization in Photorefractive Materials

Partha P. Banerjee

Department of Electrical and Computer Engineering and Center for Applied Optics, University of Alabama in Huntsville, Huntsville Alabama

Nickolai V. Kukhtarev

Physics Department, Alabama A&M University, Normal Alabama

John O. Dimmock

Center for Applied Optics and Department of Physics, University of Alabama in Huntsville, Huntsville Alabama

3.1 Introduction

It is indeed intriguing that many natural phenomena as well as the brain or animal behavioral patterns exhibit self-organization. The convective

PHOTOREFRACTIVE OPTICS
Materials, Properties and Applications

ISBN 0-12-774810-5/$30.00

rolls in a liquid when it is heated beyond the Rayleigh-Bernard instability point is an example of pattern formation in hydrodynamics due to self-organization. Here the temperature difference is the driving force or input parameter. Below the critical or threshold temperature, one can only observe random motion of the liquid particles. Besides, in an open container containing the fluid, surface tension can also affect the flow, causing tesselation of the surface and formation of hexagonal cells. Such spontaneous pattern formation is exactly what is termed self-organization, but there is no agent inside the system that does the organizing. The motion of the whole is no longer the sum of the motion of the parts, due to nonlinear interactions between the parts and the environment. Another example of pattern formation is a "wave" among spectators in a stadium — individual spectators communicate and cluster together in groups to create a nearly synchronized pattern that spreads throughout the stadium. Speaking of which, there is enough evidence that human behavioral patterns are self-organized. The human body, for example, is a complex system comprising about 10^2 joints, 10^3 muscles, 10^3 cell types, and 10^{14} neurons or neuron connections. The actions of communication, body movement etc. are the result of self-organization of this complex system pertaining to a certain control or input parameter (stimulus). In a similar fashion it has been shown that the brain itself is an active, dynamic self-organizing system. For more on the self-organizing aspects of the brain and human behavior, the readers are referred to Kelso [1], Kohonen [2], and Haken [3].

Some of the elementary concepts and conditions for self-organization are as follows [1]:

1. Patterns arise spontaneously as a result of nonlinear coupling between large numbers of interacting components.
2. The system must be far from equilibrium. Due to nonlinear interactions, energy is not distributed evenly but coalesces into patterns or flows.
3. Relevant degrees of freedom, or order parameters, must exist near nonequilibrium phase transitions, where loss of stability gives rise to new patterns and / or switching between patterns.
4. Noise must be present in the system, so that fluctuations can "feel" the system stability and provide for the system to self-organize into different patterns.

In this chapter we will discuss self-organization and its effects in optics. In fact, one of the most exciting and potentially useful areas of current research in optics involves the understanding and exploitation of self-organization in nonlinear optical systems. This self-organization may sometimes lead to the evolution of complex spatial patterns which can be regarded as the nonlinear eigenmodes of the system. Generation of these patterns is characteristically marked by the presence of intensity thresholds. The detailed study of the self-organization process, including the spatiotemporal evolution, is needed in order to harness these effects for potential practical applications.

For a long time in nonlinear optics, only problems of temporal dynamics were investigated. However, spatial distributions were only assumed, without regard to their time evolution and hence relationship with temporal instabilities. However in a nonlinear system with complicated temporal dynamics, it turns out that one cannot retain purity in spatial dimensionality. It is therefore equally important to investigate the dynamics of the transverse spatial variations which in fact give rise to very interesting patterns due to self-organization. A vast wealth of patterns can be achieved by using a nonlinear optical element with feedback that has the capability to provide for field transformation, e.g., by spatial filtering. These types of systems have been called optical kaleidoscopes, simply because of the different self-organized patterns that they can generate. Examples of nonlinear self-organized kaleidoscopic patterns are:

Rolls

Rotatory waves

Optical spirals

Hexagonal patterns

Patterns with more complicated geometry

Pattern hopping

An excellent reference for this as well as self-organization in different nonlinear optical systems is the book by Vorontsov and Miller [4].

Information processing applications of nonlinear optics are closely linked to the ability to control nonlinear optical systems which can self-organize in different ways. For instance, different patterns formed through self-organization can be used for coding and processing of optical information [4]. It has been proposed that the existence of several modes

in a laser can be used as a base for synergetic computing [5]. Fourier filtering techniques have been used in conjunction with nonlinear optical systems for information processing. Degtiarev and Vorontsov [6] used Fourier filtering in the path of a liquid crystal light valve (LCLV) system with feedback for phase distortion suppression. Such nonlinear optical systems with feedback have also been used for various kinds of pattern generation such as hexagons, rolls, etc. [7]. The dynamics of pattern formation in a coupled LCLV system with feedback have been studied by Thuring *et al.* [8].

Photoinduced scattering of laser radiation into self-organizing patterns has been observed over the past several years in a substantial number of nonlinear materials including gases and liquids [9–14]. Among solids, photorefractive materials such as $KNbO_3$ have been observed to exhibit a rich variety of such scattering including hexagonal pattern formation and rotation, as well as other patterns depending on the experimental conditions [15, 16]. Furthermore simultaneous pattern generation and self-phase conjugation have been observed due to self-organization in this material under other conditions [17, 21]. Hexagon formation has also been observed in other photorefractive materials as well, such as $BaTiO_3$ [22, 23].

Because of the richness of the scattering phenomena observed in $KNbO_3$, we anticipate that the understanding of the origins of photorefractivity and the nature of the self-organization phenomena will lead to novel and substantially enhanced nonlinear applications of this material such as set forth in the following.

1. We anticipate that the self-organization can readily be used to intelligently manufacture diffractive optical elements, such as hexagonal arrays, gratings etc. In this case, one can use the nonlinear properties of the active material to create diffractive optic elements, rather than rely on complicated geometrical processing. In the long run, these patterns can be generated and stored in thin-film photorefractive polymers. In the shorter term, one can image a plane inside of a thick crystal on a film and thereby make such diffractive elements.

2. The near-field pattern is observed to be composed of hundreds of phase-related spots in a hexagonal array which can be caused to shift or move across the face of the crystal. We believe that this can, in principle, be used for hexagonal sampling of images in digital image processing which offers spatial bandwidth savings [24]. Hexagonal array generation

has been traditionally done by fabricating binary phase gratings [25]. These hexagonal arrays can also be used to effectively couple light into a fiber bundle, which may eventually feed into adaptive antenna array structures.

3. The far-field pattern can be used to broadcast separate images of an input pattern in different directions. Further, because these separate images have specific phase relations, unique image processing can be performed by interfering these separate images with each other or with the original beam. It is also conceivable that the far-field pattern comprising six peripheral spots and the central spot can be used to monitor velocity and acceleration of a moving body.

4. As both near- and far-field pattern rotations are extremely sensitive to small misalignments of the pump beam with respect to the crystal surfaces and axes [16, 18], we anticipate that this material can be employed as an integral element in misalignment detection or rotation sensing devices.

5. The self-phase conjugation can be used to form conjugate images in both forward and backward directions without the need of complex additional optics. Edge enhancement, an important aspect of image processing, has been demonstrated using this material and there is potential to develop real-time optically edge-enhanced correlators using this concept.

6. Finally, since we can observe and measure holographic currents during grating recording in the photorefractive material [26, 27], we anticipate that the self-organization effects and their time dependencies can be modified and indeed controlled by application of external electrical fields to the $KNbO_3$ crystal. In the long term, the possibility of superposing external electrical modulation to change the holographic current and hence the diffraction pattern in the near- and far-fields seems feasible. This will open the door to exciting applications of the crystal in nonlinear information and image processing which may be electronically controllable.

Before closing this section, we would like to point out that photoinduced scattering in the $KNbO_3$ crystal has also been observed over a wide range of the visible spectrum [17]. This makes the crystals particularly attractive in low-cost applications using, for instance, portable He-Ne lasers. Not only is the understanding of self-organization important for possible applications, but also the optical and electrical measurements

on the crystal are essential in order to characterize the physical properties of the crystal related to charge transport and the nature of the nonlinearity. This will enhance the knowledge base for the crystal, useful for rigorous analysis of the self-organization phenomenon, as well as for other applications. Finally, the optical and electrical measurements can be readily used to characterize other photorefractive crystals as well.

3.2 Basic experimental observations

Self-organization leading to hexagon formation using photorefractive materials such as $KNbO_3$ can be heuristically explained as due to a photoinduced holographic scattering which develops in two stages [16]. In the first stage, scattered light is rearranged into a cone which corresponds to a Fabry-Perot mode of the nonlinear cavity formed by the refractive index mismatch at the crystal interfaces. Reflection gratings, sometimes aided by transmission gratings, may nonlinearly modify the cavity characteristic and the cone angle. At the second stage, waves scattered in the cone write new holographic gratings (second generation gratings), and those among them that have holographic grating vectors equal to the strongest gratings from the set of first generation gratings are enhanced, following a winner-take-all route. This holographic self-organization model conceptually explains the appearance of a hexagonal spot structure around the transmitted beam. Other heuristic explanations are based on the Talbot effect; this was enunciated by Tamburrini *et al.* [13] for a liquid crystal and extended to the case of $KNbO_3$ by Honda and Matsumoto [22]. Other simplified explanations of hexagon formation also exist in the literature [28]. In this case, the authors use a simplified although, maybe, unrelated model of nonlinear susceptibility in the understanding of hexagonal pattern formation in photorefractives. The detailed physics of hexagonal pattern generation in photorefractives in our opinion is complicated and not yet well understood.

$KNbO_3$ is a biaxial electrooptic material with orthorhombic symmetry and has excellent photorefractive properties marked by large beam coupling gains [29], fast buildup times, and large anisotropies [30]. Furthermore, Fe doping in $KNbO_3$ is known to increase the maximum value of the two-beam coupling gain [31]. $KNbO_3$ based phase conjugators have been implemented in various configurations [31–33] and material proper-

ties of the crystal have been extensively studied [34, 35]. The net optical nonlinearity of $KNbO_3$ has been studied using standard z-scan techniques [16, 36]. Electrical measurements have been also performed and give valuable information about the Maxwell relaxation time, screening length, and photogalvanic current [26].

Self-organization of an Ar laser single-beam scattering in a photorefractive $KNbO_3$:Fe crystal, first into a scattering cone, and then into a hexagonal pattern was observed by Honda [15] and Banerjee *et al.* [16]. Furthermore, these spots may be made to rotate about the center, and the rotation speed depends on the misalignment of the incident beam from the *c*-axis and the power of the beam. The hexagonal pattern is also influenced in real time by a low-power He-Ne laser (wavelength 632 nm): the spot pattern erases in about a second after the He-Ne laser is turned on, leaving only the scattering cone, and reappears a second after the He-Ne is turned off.

In the simplest experimental setup, an Ar laser (wavelength 514 nm) with horizontal polarization and with initial beam diameter 1 mm is reduced to a beam diameter of 0.5 mm using a confocal lens combination, and illuminates a $KNbO_3$:Fe crystal of dimensions $6 \times 6 \times 7$ mm^3 (Fig. 3.1) [16]. A slightly converging beam may also be used [15]. When the beam is normal to the incident surface, the far-field pattern is stationary in time and comprises a strong central spot with a peripheral ring which appears instantaneously, and thereafter evolves into six symmetrically spaced spots on the scattering cone (Fig. 3.2a). This far-field pattern is observed simultaneously both in the forward and backward directions; however, the diffraction efficiencies (discussed in more detail below) are not identical.

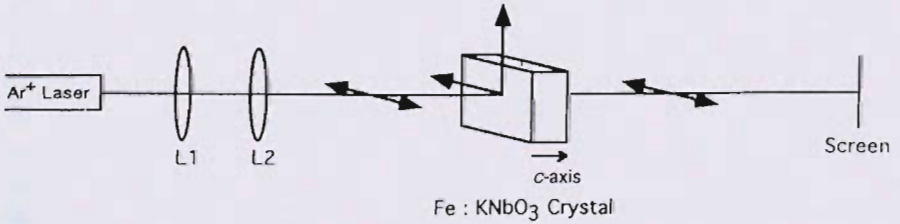

Figure 3.1: Experimental setup to observe hexagon formation in potassium niobate. (L1, L2-lenses.)

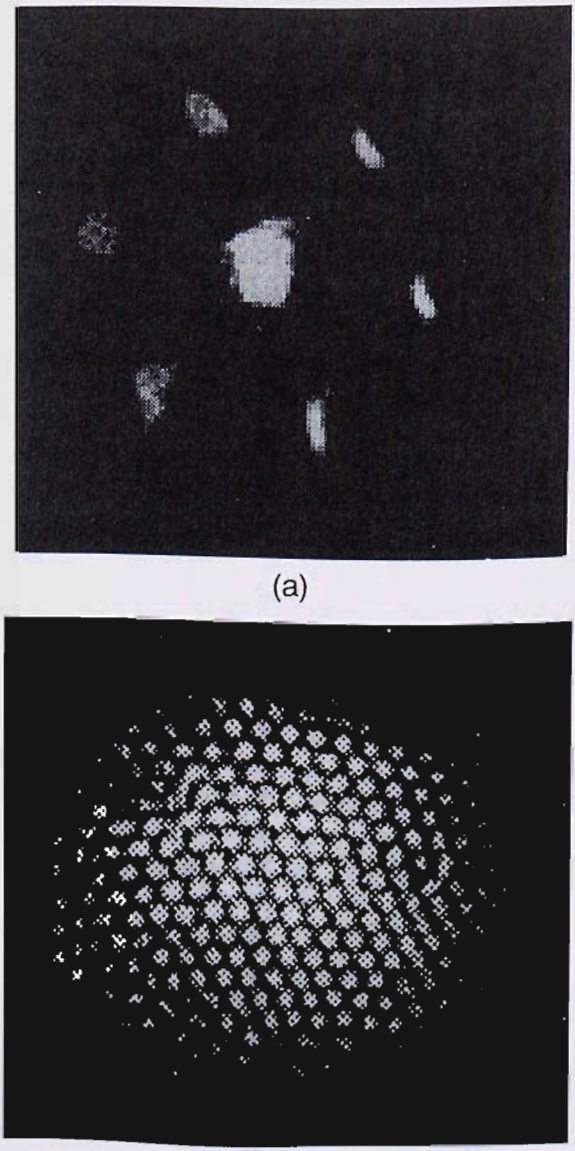

Figure 3.2: (a) Far-field transmission pattern showing central spot and hexagonal pattern. (b) Near-field pattern showing hexagonal spot array. (Source: Ref. [16]. Reprinted with permission.)

The semiangle of divergence θ of the peripheral cone is approximately 0.8° in air and is independent of the incident power. The time taken to form the spots is a few seconds for an incident power of 7.5 mW, although the spots may be formed for lower incident powers as well, with a longer formation time. The ring and all spots (central and peripheral) are also predominantly horizontally polarized. The diffraction efficiency for the spots in the forward direction is large: the intensity ratio of each transmitted peripheral spot to the transmitted central spot, which we term the forward diffraction efficiency per spot, is over 7%, for a total forward scattering efficiency into all six spots of 42%. The corresponding diffraction efficiency in the backward direction is about 4% per spot. Finally, the diffraction efficiencies seem to be relatively independent of the incident power over the range of powers investigated (7.5–30 mW).

Upon imaging different planes in the crystal (including the exit face) by a lens for the sake of visualization of the transverse nature of the optical fields, we have found, as shown in Fig. 3.2b, a periodic transverse hexagonal pattern at approximately the exit face of the crystal. Moreover, when the crystal is moved longitudinally by 0.5 cm, the same transverse pattern repeated, indicating a (nonlinearly modified) Talbot-type effect [37] (see Fig. 3.3), with contrast reversal occurring halfway between the Talbot imaging planes. The transverse period, calculated from the longitudinal period, is of the order of 30 μm, indicating a far-field diffraction angle in agreement with our observed value.

If the incident beam is slightly off-normal to the interface (typically by 0.04°), and the power is increased, the entire hexagonal pattern rotates [16]. The sense of rotation depends on the sense of the angular misalignment; thus, both clockwise and counterclockwise rotations of the pattern are possible through positive and negative angular misalignments. A typical value for the rotation speed in the steady state is 100 degrees per minute for an incident power of 30mW. The rotation speed is smaller for lower powers and smaller misalignments; however, we have observed that a minimum critical power was required to achieve constant-speed rotation in the steady state. Figure 3.4 shows the sense of rotation for various values and signs of the angular misalignment. In fact, this phenomenon of rotation may be effectively used to reconfigure the hexagonal spot array pattern to any desired orientation by increasing the beam power for a finite length of time. The existence of a minimum threshold may suggest a secondary bifurcation [38], rotation is one of the routes by which such patterns may lose stability. Rotation of the far-field could imply that

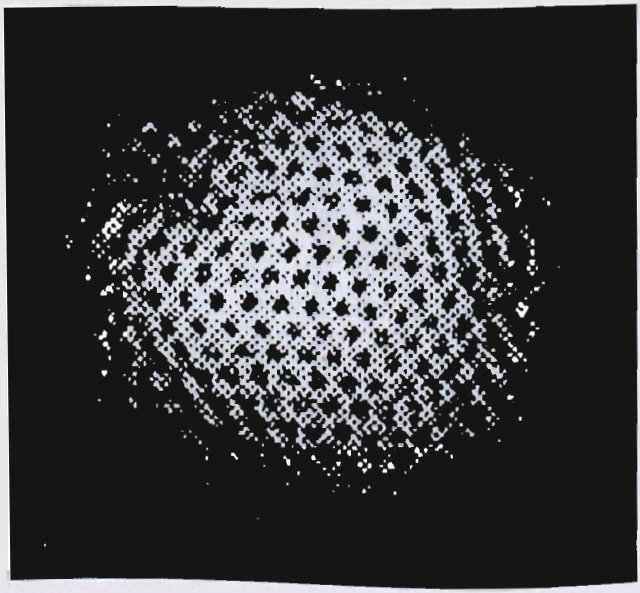

Figure 3.3: Contrast inversion of hexagonal spot array due to Talbot imaging.

individual spots in the near-field (Fig. 3.2b) undergo a change in phase as a function of time; however, this is still under investigation.

For larger angular misalignments (typically 0.3°), the far-field pattern resembles a hexagonal structure where the six spots are located on an ellipse instead of on a circle as in Fig. 3.2a. A larger misalignment (of 0.4°) destroys the hexagonal pattern altogether. What remains are two primary diffracted spots on opposite sides of the main beam orthogonal to the misalignment direction, in agreement with the experimental results of Grynberg *et al.* [9].

In related experiments, Honda obtained similar results by using a $KNbO_3$ crystal in index matching oil along with an external $BaTiO_3$ self-pumped phase conjugate mirror [15]. Also, a slightly converging beam was used, by using a convex lens of focal length 300 mm. The reflectivity of the phase conjugate mirror was about 50%. Pattern formation has also been observed using a $KNbO_3$ crystal along with a plane feedback mirror [39]. As will be discussed in the following, the angle of divergence depends on the length of the feedback path, thus it is possible to change the cone angle by adjusting the position of the external feedback mirror. In this

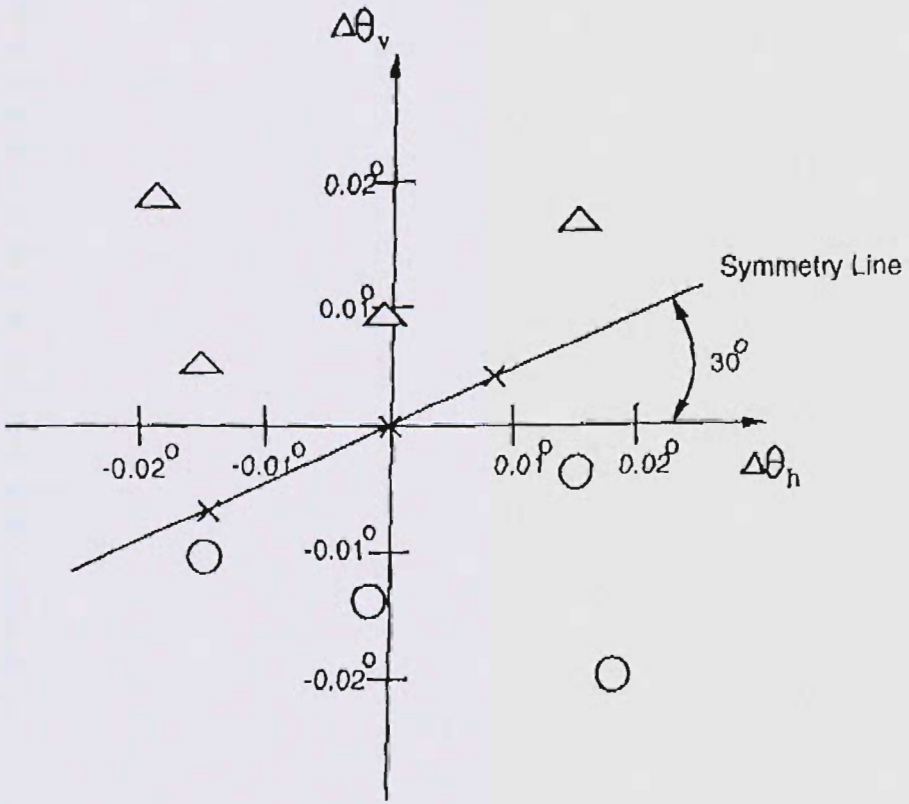

Figure 3.4: Experimental data for direction of rotation and angular misalignment. (Δ = hexagon rotates clockwise; O = hexagon rotates counterclockwise; X = hexagon is stationary.)

case, the crystal *c*-axis should be slightly tilted from the beam axis to reduce the influence of the beam reflected from the back surface of the crystal. It has been also shown that pattern rotation can be achieved by using an additional erase beam, making a small angle with respect to the direction of propagation of the pump beams in the crystal [18, 23]. The speed and sense of rotation of the hexagonal pattern in the far-field may be also controlled with the erase beam. Hexagonal pattern formation has been observed in photorefractive materials other than $KNbO_3$. Hexagonal pattern generation in Co-doped $BaTiO_3$ with an external feedback mirror

has been observed by Honda and Matsumoto [22] and by Uesu *et al.* [23]. In all of the preceding experiments, higher-order hexagonal patterns have been observed in the far-field with an increase of incident intensity. Also, interesting patterns have been observed using a single feedback system with a virtual feedback mirror. A virtual feedback mirror is achieved by inserting a lens between the exit plane of the crystal and the external feedback mirror [19, 20]. The lens images the mirror at a certain distance from the exit face of the crystal. Depending on the location of the lens, the image location could be outside or even inside the crystal. Square patterns have been observed using this arrangement. For an appropriate choice of the virtual feedback mirror (typically located inside the crystal), the hexagonal and square patterns have been shown to alternate with time, demonstrating "pattern-hopping," which is testimony to criterion #3 for self-organization in the Introduction.

In a related experiment, self-phase conjugation similar to what was observed in SBN [40] has been observed in $KNbO_3$ [17]. This configuration has applications in image processing as well, as recently shown by Banerjee *et al.* [21]. In a typical experimental setup involving $KNbO_3$: Fe [17], a wave C_1 incident at about 10° to the normal to the crystal surface is reflected from the crystal, producing C'_{-1} (Fig. 3.5). Due to scattering, additional waves C_0 and C'_0 develop, which propagate almost normal to

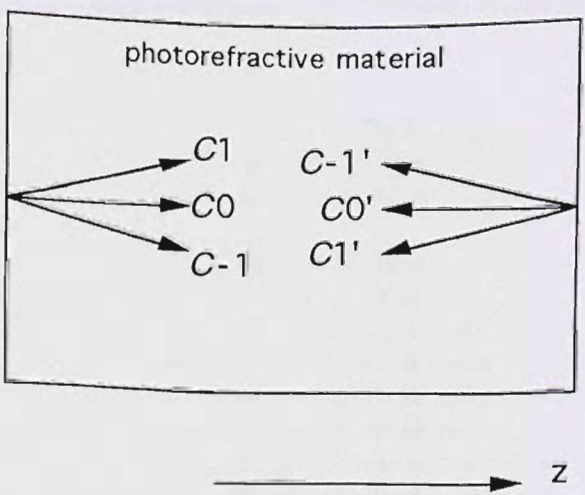

Figure 3.5: Six-wave coupling in potassium niobate.

the crystal surface. These represent concentric Fresnel rings, and are analogous to Fabry-Perot modes in a resonator. With time, the inner ring may decompose into a hexagonal pattern. Furthermore, interaction of the four waves C_0, C_0', C_1, C_{-1}' gives rise to additional waves C_{-1} (counterpropagating to C_{-1}' and phase conjugate of C_1) and C_1' (counterpropagating to C_1 and its phase conjugate).

A variation of the above experiment involves interactions initiated by two beams C_1 and C_0, and supported by reflections C_{-1}' and C_0', to eventually produce C_{-1} and C_1'. In this case we have found that if C_1 represents the field from a point source, the phase conjugate C_{-1} images a certain distance behind the photorefractive crystal. Furthermore, if C_1 is the Fourier transform of an object, the phase conjugate of the object is recovered in the far-field, traveling nominally in the direction of C_{-1}. By changing the position of the object with respect to the front focal plane of the Fourier transform lens, edge enhancement can be achieved [21].

3.3 Theory

3.3.1 Fabry-Perot modes

Assume that a radially symmetric beam $C(r)$, where r represents the radial distance in the transverse plane, is nominally normally incident onto a Fabry-Perot cavity formed by the parallel faces of the photorefractive material. The far-field intensity profile can be shown to be given by $|\hat{C}(\theta)|\, S(\theta)$, where $S(\theta)$ is a shaping function which, to a first approximation, can be shown to be

$$S(\theta) \propto \frac{1}{1 + F(\theta)\sin^2 k_0 \theta^2 L/2}. \tag{3.1}$$

Also, $\hat{C}(\theta)$ represents the Fourier transform of $C(r)$, with $\theta = k_r / k_0$, where k_r is the spatial frequency corresponding to r and k_0 is the propagation constant of the light in the medium. In the above relation F is the cavity finesse and L is the thickness of the material. From (3.1), upon setting $k_0\theta^2 L/2 = \pi$, the semiangle of the first ring can be calculated to be approximately 0.4° in the material, which is of the order of our observed value of 0.8° in air. With time, the ring may break up into hexagonal spots, as observed experimentally. Note also that in the experiments, secondary (or higher-order diffraction) rings, and sometimes higher-order

hexagonal spots, are also observed. We have observed in our experiments that the radius of the second ring is observed to be $\sqrt{3}$ times that of the first, which can be also derived from (3.1) by setting $k_0\theta^2 L/2 = 3\pi$.

We would like to point out that the existence of Fabry-Perot modes in the crystal cavity supports the concept of periodic imaging during propagation in the crystal. In so-called "open" cavities consisting of a matched or misaligned photorefractive crystal and an external feedback mirror, the concept of Talbot imaging has been used to determine the scattering angle [22, 23]. However we feel that the concept of Talbot imaging as discussed in [22, 23] can only be applied to the case of propagation in the "cavity" between a "thin" slice of the photorefractive material containing the induced reflection grating and the external mirror. More on this is discussed in the following.

In a nonlinear system where the incident beam may originate from light scattering, the coupling between forward and backward traveling waves may be provided by transmission and/or reflection gratings. From experimental results on beam coupling, it has been shown that reflection gratings are dominant. In the remainder of this chapter, we will assume only reflection gratings to be present. It turns out that the scattering angle will be nonlinearly modified depending on the strength of the reflection grating.

3.3.2 Model equations

We represent the forward and backward traveling waves in the nonlinear photorefractive material as

$$E = \mathrm{Re}[(C_e \exp - jk_0 z + C_{e'} \exp jk_0 z) \exp j\omega_0 t] \tag{3.2}$$

where $C_{e,e'}$ denote the forward and backward traveling wave amplitudes, respectively, and ω_0 is the angular frequency of the light in the medium. We also assume that the material has light-induced changes in the refractive index due to reflection gratings formed in the material, with spatial frequency $2k_0$. The spatial evolution of the forward and backward traveling envelopes can be then written as

$$\begin{aligned} L_e C_e &= -jk_0 \delta n C_{e'}, \\ L_{e'} C_{e'} &= -jk_0 \delta n^* C_e, \end{aligned} \tag{3.3}$$

where $L_{e,e'}$ are linear operators given by the relation

$$L_{e,e'} = \partial/\partial z \mp j(1/2k_0)\nabla_\perp^2. \tag{3.4}$$

The variable δn represents the fractional change of refractive index due to the induced reflection grating and evolves according to

$$\tau \partial \delta n / \partial t + \delta n = \gamma \frac{C_e C_{e'}^*}{|C_e|^2 + |C_{e'}|^2}. \tag{3.5}$$

We consider reflection gratings only for now because they are dominant in photorefractive potassium niobate [15]. Transmission gratings have been assumed in other analyses, such as for the determination of the onset of instability [41]. By using the model of excitation of satellite beams due to propagation of contrapropagating primary or pump beams, and transmission gratings, so-called *spatial dispersion curves* for the onset of instabilities leading to satellite beam formation have been derived. The plots show the dependence of the minimum threshold gain as a function of the angle between the pump and the spatial sidebands [41]. Dispersion curves assuming predominantly transmission gratings and aided by reflection gratings have been also derived by Kukhtarev *et al.* [17]. Later on in the chapter, we will provide the results of such dispersion curves but using reflection gratings in the model, since it pertains more closely to spontaneous pattern generation in photorefractive potassium niobate.

We would like to point out that pattern dynamics have been extensively studied in a bidirectional photorefractive ring resonator assuming transmission grating approximation and four-wave mixing in the active photorefractive medium [42]. Spontaneous symmetry breaking, dynamical oscillations, vortex formation and complex pattern development are predicted for large Fresnel numbers. A photorefractive oscillator with a stable resonator has been used to model a nonlinear dynamical system in which transverse mode patterns have been observed [43].

3.3.3 Instability criterion and the dispersion relation

There is considerable work done on the onset of instabilities in a photorefractive medium with reflection gratings due to counterpropagation of pump beams. The analysis of Sturman and Chernykh [44] assumes a medium in which there is no energy coupling. Saffman *et al.* [45] has performed a more detailed analysis assuming both real and complex coupling coefficients. Honda and Banerjee [39] have improved on their analysis, by showing that pattern generation can occur even for purely energy coupling.

We now present the threshold condition for instabilities derived for the experimental arrangement in [39] with the photorefractive crystal and a feedback mirror. We use the relations in Eqs. (3.3)–(3.5) and substitute

$$C_{e,e'} = C_{0,0'}[1 + c_{1,1'}\exp -jK\cdot r + c_{-1,-1'}\exp jK\cdot r], c_{i,i'} = C_{i,i'}/C_{0,0'} \tag{3.6}$$

where K is the transverse wavenumber and r denotes the transverse coordinate to get

$$\begin{aligned}
(\partial/\partial z - jk_d)c_1 &= jA\gamma(c_1 + c_{-1}{}^* - c_{1'} - c_{-1'}),\\
(\partial/\partial z + jk_d)c_{-1}{}^* &= -jA\gamma^*(c_1 + c_{-1}{}^* - c_{1'} - c_{-1'}),\\
(\partial/\partial z + jk_d)c_{1'} &= jA\gamma^*(c_1 + c_{-1}{}^* - c_{1'} - c_{-1'}),\\
(\partial/\partial z - jk_d)c_{-1} &= -jA\gamma(c_1 + c_{-1}{}^* - c_{1'} - c_{-1'}),
\end{aligned} \tag{3.7}$$

where $k_d = K^2/2k_0$ and $A = A(z) = |C_0|^2\,|C_{0'}|^2/[|C_0|^2 + |C_{0'}|^2$. Note that since A is a function of z, Eqs. (3.7) cannot be solved analytically. However, when the reflectivity of the feedback mirror is unity or the reflection from the back surface of the crystal is considerable, we can approximate $A \sim 1/4$ [39].

For the case of a feedback mirror placed behind the crystal, the boundary conditions can be written as

$$\begin{aligned}
&c_{1,-1}(0) = 0,\\
&c_{1'}(L) = \exp(-2jk_d l)c_1(L), c_{-1'}(L) = \exp(2jk_d l)c_{-1}{}^*(L)
\end{aligned} \tag{3.8}$$

where L is the crystal thickness and l denotes the distance between the photorefractive medium and the feedback mirror. The threshold condition can be found using (3.7) and (3.8) and using the Laplace transformation to solve. Assuming that the mirror is placed against the back surface of the crystal, the "dispersion relation" can be written as

$$\begin{aligned}
\cos wL\cos k_d L + (\gamma/2w)\sin wL\cos k_d L\\
+ (k_d/w)\sin wL\sin k_d L = 0,
\end{aligned} \tag{3.9}$$

where we have assumed the coupling constant γ to be purely imaginary ($\gamma \to -j\gamma$) and $w^2 = k_d^2 - \gamma^2/4$. Figure 3.6 shows the dispersion curve for this case. When γ is just above the threshold for spatial sideband generation, the direction of the sidebands will correspond to k_d which gives the minimum of the dispersion curve. For other mirror locations the angle between the carrier and the spatial sidebands decreases as shown in [23, 39].

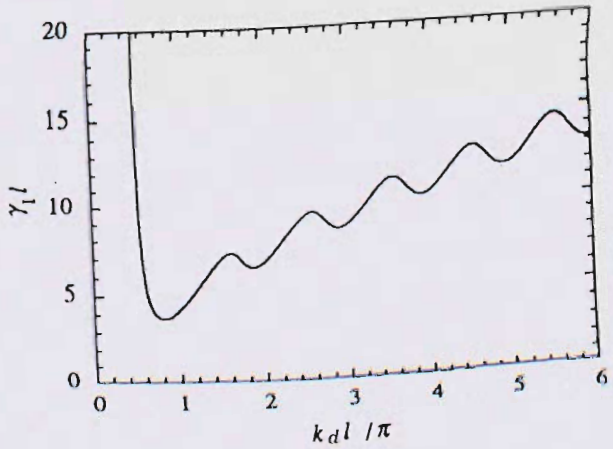

Figure 3.6: Threshold condition assuming purely energy coupling and for mirror feedback. Mirror is located at the back surface of the sample. (Source: Ref. [39]. Reprinted with permission.)

3.3.4 Nonlinear eigenmodes in the steady state

The formulation stated above through Eqs. (3.3–3.5) can also be used to study the exact spatial behavior of the carriers (contrapropagating pumps) and the spatial sidebands. In the steady state, the spatial evolution of the carriers and the spatial sidebands lying on a scattering ring can be studied by solving the system of equations [46–48]

$$L_i C_i = \sum_{j'} \delta n_{ij'} C_{j'} = \gamma \sum_{j'kl'} C_k C_l^* C_{j'} \Big/ \left[\left| \sum_i C_i \right|^2 + \left| \sum_i C_{i'} \right|^2 \right] \tag{3.10}$$

$$L_{i'} C_{i'} = \sum_j \delta n_{ji'}^* C_j = \gamma^* \sum_{j'kl'} C_k C_{l'}^* C_j \Big/ \left[\left| \sum_i C_i \right|^2 + \left| \sum_i C_{i'} \right|^2 \right]$$

where we have assumed the optical properties of the photorefractive material to be isotropic. As seen from Eq. (3.10), coupling will occur only between waves whose transverse wavevectors satisfy the general relation $K_i + K_{l'} = K_k + K_{j'}$. An example of a set of contrapropagating pumps and a set of six forward and backward propagating scattered sidebands is shown on the transverse $\boldsymbol{K}$-plane in Fig. 3.7. It can be shown that seven different types of couplings may occur. For example, $K_{l'} = 0$, $K_i = K_k + K_{j'}$ couples the main forward traveling beam with three waves that are

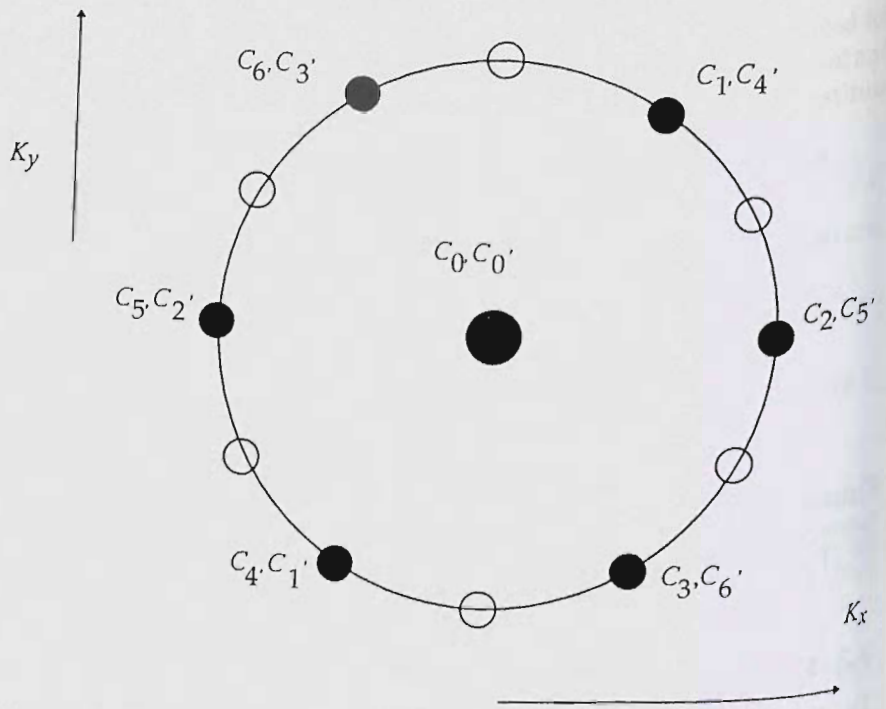

Figure 3.7: Transverse **k**-vectors of hexagonally related scattered waves with regard to that of the forward- and backward-propagating beams. Two sets of hexagonally related scattered beams are shown.

hexagonally related. The interaction $K_i = -K_{i'}$, $K_k = -K_{j'}$ couples sets of hexagonally related waves together.

In what follows, we assume a geometry identical to the experimental arrangement in [16] with only the unmatched crystal and no feedback mirror. Using Eq. (3.10) as a model, the spatial evolution of the carriers and the sidebands have been analyzed for the case when there are 72 sidebands symmetrically distributed on the scattering ring [47, 48]. The preliminary results which were performed using a purely imaginary γ shows the general nature of the "modes" in the steady state that can exist within the interaction region in the photorefractive material. These modes show the permissible values of the phase difference between the pump and the sidebands at the front surface of the material for different values

of the gain parameter proportional to γ. Furthermore, one can simultaneously get the spatial variations of the contrapropagating pumps and the spatial sidebands, assumed equal in magnitude for simplicity. The results therefore define the conditions needed for self-organization of the laser beam into a scattering ring, starting from fanning noise in the material. However, it turns out that the ratio of scattered to pump intensities both in the forward and the backward directions are not exactly similar to experimentally observed results [16].

We would like to point out that a simple time evolution simulation to illustrate the basic principle of the formation of the scattering ring and hexagon formation can be performed by starting from the model shown in Eqs. (3.3)–(3.5) and even assuming a constant (intensity independent) imaginary coupling constant, constant amplitudes for the interacting pumps and spatial sidebands in the photorefractive material, and assuming a thin sample [46]. Taking an initial linear scattering from beam fanning, the evolution of the spatial sidebands into a scattering cone and eventually into hexagonal pattern in the far-field is shown in Fig. 3.8.

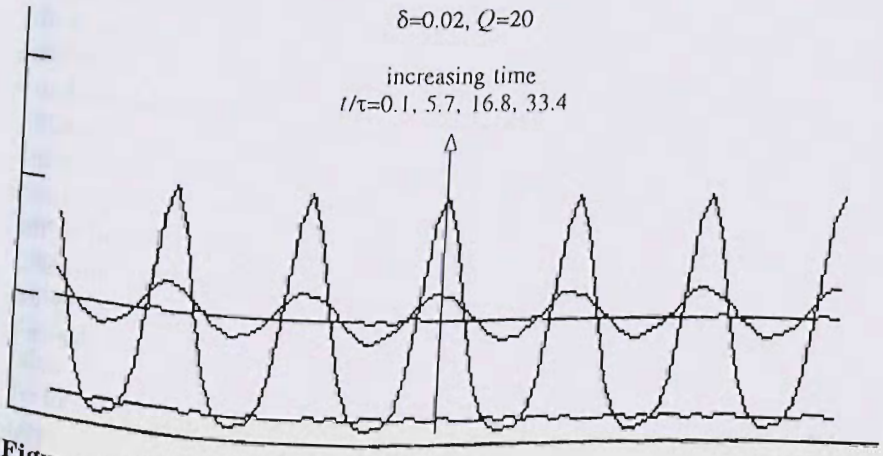

Figure 3.8: Time evolution of scattering around a circle, showing the growth of the scattering ring and eventual formation of the hexagonal spot pattern. The normalized coupling parameter Q showing coupling between hexagonally related points on the scattering ring and the pump is taken to be 20, and the linear scattering coefficient δ from the pump (to initiate the self-organization process) is taken to be 0.02 [46].

The plots show that the energy scattered into the ring as the first stage of the self-organization process essentially later redistributes into the hexagons. The plots are quantitatively modified slightly if transmission gratings are also incorporated into the simulations. All simulation results are in qualitative agreement with experimental observations [16]. If one monitors the minimum value of the gain needed for the onset of instabilities as a function of the linear scattering parameter, it is observed that the threshold gain decreases sharply with increasing initial linear scattering, as expected, and tends to slightly decrease for very high values of the scattering parameter. This decrease can be attributed to the fact that excessive linear scattering tends to deplete the pumps of their initial energy, thus inhibiting the formation of reflection gratings and eventual transfer of pump energies into the spatial sidebands. This simple simulation also demonstrates the justification for looking for exact spatial eigenmodes which depict the spatial variation of the pumps and the scattering ring as the first stage of the self-organization process.

As stated in the preceding discussion, the discrepancy between numerical simulations for the nonlinear eigenmodes and experimental results of the energy scattered into the ring and eventually into the hexagon can be resolved by assuming a complex coupling constant. Possible reasons for the nonideal phase of the coupling coefficient are as follows. As in any photorefractive material, the contribution to photorefractivity can come from both diffusion and photovoltaic contributions. While diffusion creates a space-charge field which is out of phase with the intensity profile, photovoltaic effects give rise to space-charge fields which are in phase with the intensity [49]. In general, therefore, an arbitrary phase difference may exist. Furthermore, even for a purely photovoltaic material, it has been shown that there can exist a phase difference between the intensity grating and the fundamental spatial frequency component of the space-charge field, for large modulation depths. This can also give rise to a complex coupling coefficient [50].

Starting from Eq. (3.10) and setting $\gamma \rightarrow \gamma \exp j\phi$ with

$$C_{i,i'} = S_{i,i'}(z)\exp(-jK_{i,i'} \cdot r)\exp(\mp j\pi z / L)\exp(j\phi_{i,i'}(z)) \qquad (3.11)$$

we can derive the spatial evolution equations for the amplitudes and phsaes of the interacting waves. If we assume that the amplitudes and phases $S_{i,i'}$, $\phi_{i,i'}$, $i,i' \neq 0$ of the interacting waves on the scattering ring are

identical for simplicity, we get after extensive algebra, coupled differential equations which have the functional forms [51]

$$\begin{aligned} \partial S_0^2/\partial z &= (\gamma/I)F_0[S_0^2,S_1^2,S_{0'}^2,S_{1'}^2,b,c,\phi,N] - N\delta S_0^2, \\ \partial S_1^2/\partial z &= (\gamma/I)F_1[S_0^2,S_1^2,S_{0'}^2,S_{1'}^2,b,c,\phi,N] + \delta S_0^2, \\ \partial b/\partial z &= (\gamma/I)F_b[S_0^2,S_1^2,S_{0'}^2,S_{1'}^2,b,c,\phi,N] + \pi/L, \end{aligned} \tag{3.12}$$

where

$$b = \phi_{1'} - \phi_{0'} + \pi z/L, c = \phi_1 - \phi_0 - \pi z/L \tag{3.13}$$

The corresponding equations for $S_{0',1'}^2$, c can be found by interchanging the primed and unprimed variables, interchanging b and c in the above equations and replacing L by $-L$. In Eq. (3.12), I is the incoherent intensity and we should point out that Eq. (3.12) is valid assuming up to third-order interactions. The constant δ is a linear scattering parameter. N is the number of interacting waves on the scattering ring, taken here to be equal to 72. The exact expressions for F_i in (3.12) are given in [47, 48, 51]. Conservation rules for waves interacting through the formation of reflection gratings hold, and Eq. (3.12) is solved numerically assuming boundary conditions pertinent to the front and back surfaces of the crystal which generate the counterpropagating waves in a truly mirrorless configuration.

The numerical results (not shown here) show the existence of multiple eigenmodes which are possible in the photorefractive medium. Each eigenmode is characterized by a value of $b(0)$ [assumed equal to $c(0)$] and ϕ, and is the locus of permissible solutions on the $b(0) - \phi$ plane. If the forward and backward scattering ratios, defined as the fraction of the pump energy scattered onto the ring, are monitored, it follows that by relaxing the condition on ϕ, namely, making it arbitrary, it is possible to attain values similar to experimental observations. For instance, for a value of $\phi = 230°$, about 40% of the energy is scattered into the ring in the forward direction, with about 30% in the backward direction, in close agreement with experimental observations [16]. The fact that a complex coupling constant is required to achieve the expected forward and backward scattered energies corroborates the fact that the ideal phase difference (namely 270°) between the intensity grating and the induced refractive index profile is probably changed due to contributions from diffusion from the finite modulation depth of the intensity grating, as

explained in the preceding discussion. The phase difference between the pump and the sidebands at the front surface is close to 270° for this case, which implies phase modulation of the profile of the total beam at this plane (and also at the exit plane), with amplitude modulation in the center of the photorefractive material. The analysis also enables us to track the exact spatial evolution of the pumps and the spatial sidebands; this is shown in Fig. 3.9. We would also like to point out that agreement between theory and experiment is only observed for the above value of ϕ, which explains why self-organization is not observed when the experiment is performed with the c-axis of the crystal turned in the reverse direction [16].

Finally we would like to point out other related analytical work in the area of transverse instabilities. The effect of crystal symmetry on the

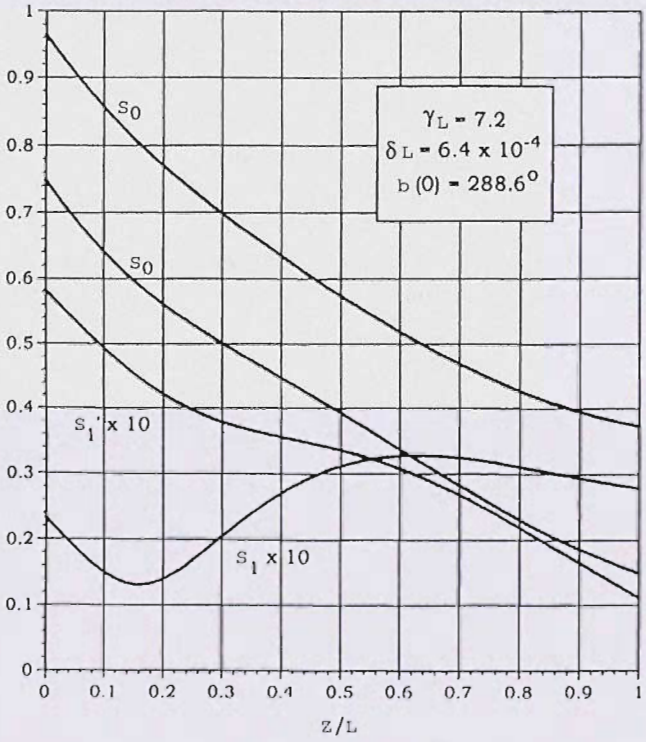

Figure 3.9: Spatial variation of the forward- and backward-scattered and main beam amplitudes during propagation through the crystal.

formation and rotation of hexagonal scattering patterns in photorefractive materials has been discussed by Dimmock [52].

For the orthorhombic, C_{2v}, symmetry of the $KNbO_3$ crystal, the two crystallographic planes perpendicular to the a- and b-axes are planes of reflective symmetry and the c-axis is a two-fold rotation axis. If we consider that the incident laser beam in Fig. 3.1 is polarized along the a-axis, and that the laser beam, and its reflected beams are directed exactly along the c-axis, then the experiment will also possess the C_{2v} symmetry. Namely, it is invariant with respect to twofold rotations about the c-axis, and reflections in the two symmetry planes. Such a configuration can show no right- or left-handedness. The constraints of symmetry on the possible rotations are shown in Fig. 3.10. Let K_x and K_y represent the transverse K vectors of the laser beam with respect to the crystallographic c-axis direction. If the crystal reflection planes are perpendicular to the c-axis then K_x and K_y are proportional to $\Delta\theta_h$ and $\Delta\theta_v$. If the laser beam propagates parallel to either of the two symmetry planes the orthorhombic symmetry is preserved and no rotation can occur. It is only when the laser beam propagates in a direction corresponding to one of the four quadrants that predictable and stable rotation is allowed. Figure 3.4 shows how the direction of rotation experimentally depends on the beam direction. This is not exactly what is predicted in Fig. 3.10. The discrepancy can be explained by postulating additional asymmetries in the material, and

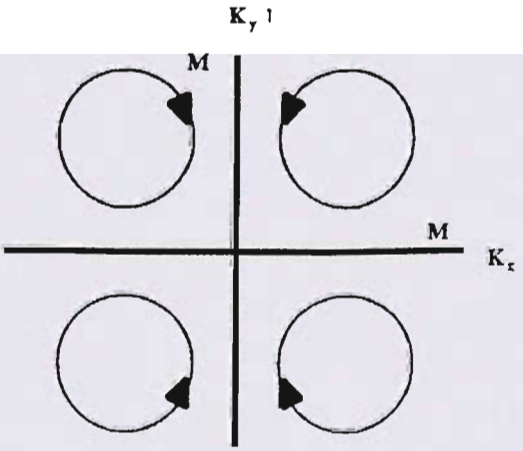

Figure 3.10: Dependence of rotational sense on beam direction.

misorientations of the front and back surfaces with respect to the *c*-axis of the crystal. The effect of orthorhombic anisotropies of the index of refraction and the electrooptic coefficients has been discussed in detail in [52].

Sandfuchs *et al.* have determined the instability criteria for the case when a voltage is applied across the photorefractive material, and assuming reflection gratings and finite modulation index for the intensities [53]. For related work in Kerr media, the reader is also referred to [54–56].

3.3.5 Self-phase conjugation

As described in Section 3.2, interactions initiated by incident beams $C_{0,1}$ and supported by internal reflections $C_{0',-1'}$ eventually generate $C_{-1,1}$ [17]. Using equations analogous to Eq. (3.10) for the interfering waves and in the steady state we can write, approximately [46],

$$L_e C_{-1} \approx n_{0,-1'} C_0', L_e' C_1' \approx n_{0',1} C_0, \qquad n_{0,-1'} \propto \gamma C_0 C_1'^*, n_{0',1} \propto \gamma C_0' C_1^*. \tag{3.14}$$

Using the preceding relations, the phase conjugate intensities $I_{-1,1'}$ can be found as

$$I_{1'} \propto TRI_{1inc} I_{0inc}^2{}^2/(1+R)^2(I_{1inc}+I_{0inc})^2; I_{-1} \propto RI_{1'} \tag{3.15}$$

where $I_{1inc,0inc}$ are the input intensities of the waves 1 and 0; T and R represent the transmittivity and reflectivity of the interface, respectively. The derivation above can be modified to include the effects of transmission gratings as well. A detailed description of the evolution of the conjugates is important and will be performed in the future, especially in light of recent experimental observations that the time dynamics of the different phase conjugates formed are different and could hence originate from transmission or reflection gratings.

3.3.6 Model of hexagonal formation based on transverse electrical instability

In what follows, we will discuss the contribution of electrical instabilities to the formation of hexagonal structures. An adequate description of self-organized pattern in $KNbO_3$ and other thick photorefractive materials includes material equations (like diffusion-drift model) and Maxwell's

equations. Both material and optical equations are nonlinear and are potentially capable of describing formation of spatial-temporal patterns. As an example, we can mention the problem of the holographic subharmonic [57], observed during self-diffraction of two beams with slightly different frequencies, and with an external electric field in $Bi_{12}SiO_{20}$ crystals. The appearance of an additional beam between intersecting "pump beams" was originally explained by optical nonlinearities [58]. Later it was realized that instabilities of material equations, like period doubling, may lead to formation of a subharmonic component in the space-charge field and in the refractive index [59]. Similar trends are visible in the explanation of hexagon patterns in the thick photorefractive materials.

All previous explanations of pattern formation in photorefractive crystals were based on instabilities of optical equations (Maxwell's equations) where material equations play only an insignificant role. Only recently it was realized that photogalvanic currents may be responsible for contrast enhancement, and may result in space-charge instabilities [50]. Quantitatively, formation of the spatial patterns due to photogalvanic current may be explained taking into account the relation $\nabla \cdot J = 0$. This equation implies that the current has a vortex structure and forms closed loops. Detailed calculations of the transversal structure caused by photogalvanic nonlinearity is beyond the scope of this discussion. The ansatz that photogalvanic instabilities lead to transverse patterns of the E-field and refractive index lets us discuss experimental results in the near field.

Transversal modulation of the refractive index of a thick photorefractive crystal may be regarded as recording of a bunch of optical channels or waveguides. As was shown in [60], modulation of the refractive index may be visualized in the near-field as optical channeling. We can thus model the transversal modulation of the dielectric constant by the function

$$\varepsilon(x,y) = \varepsilon_0 + \varepsilon_x \cos K_x x + \varepsilon_y \cos(K_y y + \varphi) \tag{3.16}$$

where ε_0 denotes the average value of the permittivity, and $\varepsilon_{x,y}$ are the amplitudes of the modulation along the transverse x- and y-axis, with wave numbers K_x, K_y and proper phase shift φ. Introducing the function $\varepsilon(x,y)$ in Maxwell's equations, we can get the following result for the near-field intensity:

$$\begin{aligned} I(x,y) = I_0[1 &+ \varepsilon_x(L_x/\lambda)^2 \sin^2(\pi\lambda z/2L_x^2)\cos K_x x \\ &+ \varepsilon_y(L_y/\lambda)^2 \sin^2(\pi\lambda z/2L_y^2)\cos(K_y y + \varphi)] \end{aligned} \tag{3.17}$$

where $L_{x,y} = 2\pi / K_{x,y}$ and λ is the wavelength. The solution [Eq. (3.17)] is valid for small modulation and includes longitudinal modulation with the periods

$$z_{x,y} = 2L_{x,y}^2 / \lambda . \tag{3.18}$$

We can see that Eq. (3.17) also describes contrast inversion. As described before, for experimental values with $KNbO_3$ ($\lambda = 0.514$ μm, $L_x = L_y = 30$ μm), we can get for longitudinal period $z_x = z_y = 0.49$ cm that is close to the experimental value of 0.5 cm [16].

We would like to reiterate that the explanation of hexagonal structures by Talbot effect imaging is valid only for optically thin gratings, where Talbot effect description during propagation in free-space is justified. In our case we have used a thick crystal (1 cm thick) and we should use an adequate model of thick holographic gratings. The channeling effect is pronounced for thick gratings, and naturally describes the effect of contrast inversion. In contrast to Bragg diffraction that normally needs coherent light, channeling may be observed also in incoherent illumination.

3.5 Conclusion

We have summarized, using minimal mathematics, some important aspects of an area which is complicated for two reasons: (1) because of the nonlinear and spatiotemporal nature of the problem, and (2) because the response of a photorefractive material to incident light is a complicated phenomenon, governed by a set of nonlinear coupled differential equations. Wherever possible, experimental results have been quoted or referred to to assure readers that there is some connection to reality behind the complicated mathematics. The list of potential applications given in the Introduction is also meant to excite the reader to future possibilities. We hope the summary of self-organization in photorefractives, as presented, will interest readers to undertake the challenging and unfinished work in the area. Finally, we have tried to compile the important references in the general area, and although undoubtedly some have been left out for brevity and due to oversight, cross-referencing should prove valuable in finding all necessary citations to this rapidly growing field.

Acknowledgment

P. P. B. thanks Prof. K. Matsushita of Osaka City University for his help during preparation of the manuscript. P. B. B. also acknowledges collaboration with Drs. T. Honda (NRLM, Tsukuba, Japan), F. Madarasz (CAO, UAH), and H-L Yu.

References

1. J. A. Scott Kelso, *Dynamic Patterns: The Self Organization of Brain and Behavior*, MIT Press, Cambridge MA, 1995.
2. T. Kohonen, *Self-organization and Associative Memory*, Springer-Verlag, New York, 1984.
3. H. Haken, *Advanced Synergetics: instability hierarchies of self-organizing systems and devices*, Springer-Verlag, New York, 1983.
4. M. A. Vorontsov and W. B. Miller, *Self-Organization in Optical Systems and Applications in Information Technology*, Springer, Berlin, 1995.
5. A. Fuchs and H. Haken, *Neural and Synergistic Computers*, Springer, Berlin, 1988.
6. E. V. Degtiarev and M. A. Voronotsov, "Spatial filtering in nonlinear two-dimensional feedback systems: phase distortion suppression," *J. Opt. Soc. Amer.*, **B12**, 1238, 1995.
7. M. A. Vorontsov and W. J. Firth, "Pattern formation and competition in nonlinear feedback systems with two-dimensional feedback," *Phys. Rev.*, **A49**, 2891, 1994.
8. B. Thuring, A. Schreiber, M. Kreuzer and T. Tcshudi, "Spatio-temporal dynamics due to competing spatial instabilities in a coupled LCLV feedback system," *Physica*, **D96**, 282, 1996.
9. G. Grynberg, E. LeBihan, P. Verkerk, P. Simoneau, J. R. Leite, D. Bloch, S. LeBoiteux and M. Ducloy, "Observation of instabilities due to mirrorless four-wave mixing oscillations in sodium," *Opt. Comm.*, **67**, 363, 1988.
10. J. Pender and L. Hesselink, "Degenerate conical emission in atomic sodium vapor," *J. Opt. Soc. Amer.*, **B7**, 1361, 1990.
11. G. Grynberg, A. Maitre and A. Petrosian, "Flowerlike patterns generated by a laser beam tansmitted through a rubidium cell with a single feedback mirror," *Phys. Rev. Lett.*, **72**, 2379, 1994.

12. B. Thuring, R. Neubecker and T. Tschudi, "Transverse pattern formation in an LCLV feedback system," *Opt. Comm.*, **102**, 111, 1993.

13. M. Tamburrini, M. Bonavita, S. Wabnitz and E. Santamato, "Hexagonally patterened beam filamentation in a thin liquid crystal film with a single feedback mirror," *Opt. Lett.*, **18**, 855, 1993.

14. J. Gluckstad and M. Saffman, "Spontaneous pattern formation in a thin film of bacteriorhodopsin with mixed absorptive nonlinearity," *Opt. Lett.*, **20**, 551, 1995.

15. T. Honda, "Hexagonal pattern formation due to counterpropagation in $KNbO_3$," *Opt. Lett.*, **18**, 598, 1993.

16. P. P. Banerjee, H-L Yu, D. A. Gregory, N. Kukhtarev, and H. J. Caulfield, "Self-organization of scattering in photorefractive $KNbO_3$ into a reconfigurable hexagonal spot array," *Opt. Lett.*, **20**, 10, 1995.

17. N. Kukhtarev, T. Kukhtareva, P. P. Banerjee, H-L Yu and L. Hesselink, "Broad-band, dynamic, holographically self-recorded, and static hexagonal scattering patterens in photorefarctive $KNbO_3$," *Opt. Engr.*, **34**, 2261, 1995.

18. T. Honda, "Flow and controlled rotation of the spontaneous optical hexagon in $KNbO_3$," *Opt. Lett.*, **20**, 851, 1995.

19. T. Honda, H. Matsumoto, M. Sedlatschek, C. Denz and T. Tschudi, "Spontaneous formation of hexagons, squares and sqeezed hexagons in a photorefractive phase conjugator with virtually internal feedback mirror," *Opt. Comm*, **133**, 293, 1997.

20. C. Denz, M. Schwab, M. Sedlatschek, T. Tschudi and T. Honda, "Pattern dynamics and competition in a photorefractive feedback system," *J. Opt. Soc. Amer.*, **B15**, 2057, 1998.

21. P. P. Banerjee, H-L Yu, D. A. Gregory and N. Kukhtarev, "Phase conjugation, edge detection and image broadcasting using two-beam coupling configuration in photorefractive $KNbO_3$:Fe," *Opt. and Laser Tech.*, **28**, 89, 1996.

22. T. Honda and H. Matsumoto, "Buildup of spontaneous hexagonal patterens in photorefarctive BaTiO3 with a feedback mirror," *Opt. Lett.*, **20**, 1755, 1995.

23. Y. Uesu, A. Ueno, M. Kobayashi and S. Odoulov, "Hexagon formation in photorefractive crystals as mirrorless coherent oscillation," *J. Opt. Soc. Amer.*, **B15**, 2065, 1998.

24. R. Mersereau, "The processing of hexagonally sampled two-dimensional signals," *Proc. IEEE*, **67**, 930, 1979.

25. N. C. Roberts, A. G. Kirk and T. J. Hall, "Binary phase gratings for hexagonal array generation," *Opt. Comm.*, **94**, 501, 1992.

26. N. Noginova, N. Kukhtarev, T. Kukhtareva, M. Noginov, H. J. Caulfield, P. Venkateswarlu, D. Parker and P. P. Banerjee, "Photoinduced electric current in Fe doped $KNbO_3$," *J. Opt. Soc. Amer.* **B14**, 1390, 1997.

27. P. Bernasconi, I. Biaggio, M. Zgonik and P. Gunter, "Anisotropy of electron and hole drift mobility in $KNbO_3$ and $BaTiO_3$," *Phys. Rev. Lett.*, **78**, 106, 1997.

28. W. J. Firth in *Self-Organization in Optical Systems and Applications in Information Technology*, M. A. Vorontsov and W. B. Miller (eds.), Springer, Berlin, 1995.

29. C. Medrano, E. Voit, P. Amrhein and P. Gunter, "Optimization of photorefractive properties of $KNbO_3$ crystals," *J. Appl. Phys.*, **64**, 4668, 1988.

30. E. Voit, M. Z. Zha, P. Amrhein and P. Gunter, "Reduced $KNbO_3$ crystals for fast nonlinear optics," *Appl. Phys. Lett.*, **51**, 2079, 1987.

31. C. Medrano, M. Zgonik, S. Berents, P. Bernasconi and P. Gunter, "Self-pumped and incoherent phase conjugation in Fe doped $KNbO_3$," *J. Opt. Soc. Amer.*, **B11**, 1718, 1994.

32. C. Medrano, M. Ingold and P. Gunter, "Self-pumped optical phase conjugation and light oscillation in Fe doped $KNbO_3$," *Opt. Comm.*, **77**, 411, 1990.

33. G. Pauliat and P. Gunter, "Coherent light oscillations with photorefractive $KNbO_3$ crystals," *Opt. Comm.*, **66**, 329, 1988.

34. M. Zgonik, K. Nakagawa and P. Gunter, "Electrooptic and dielectric properties of photorefractive $BaTiO_3$ and $KNbO_3$," *J. Opt. Soc. Amer.*, **B12**, 1416, 1995.

35. C. Medrano, M. Zgonik,, N. Sonderer, C. Beyler, S. Krucker, J. Seglins, H. Wuest and P. Gunter, "Photorefractive effect in Cu and Ni doped KNbO3 in the visible and near infra-red," *J. Appl. Phys.*, **76**, 5640, 1994.

36. Q. W. Song, C. P. Zhang and P. J. Talbot, "Anisotropic light induced scattering and position dispersion in a $KNbO_3$:Fe crystal," *Opt. Comm.*, **98**, 269, 1993.

37. J. W. Goodman, *Introduction to Fourier Optics*, 2nd ed. McGraw-Hill, New York, 1996.

38. F. Papoff, G. D. Alessandro, G. L. Oppo and W. J. Firth, "Local and global effects of boundaries on optical pattern formation in Kerr media," *Phys. Rev.*, **A48**, 634, 1993.

39. T. Honda and P. P. Banerjee, "Threshold for spontaneous pattern formation in reflection grating dominated photorefractive media with mirror feedback," *Opt. Lett.*, **21**, 779, 1996.

40. N. Bogodaev, Y. Kuzminov, N. Kukhtarev and N. Polozkov, "Photoinduced adaptive mirror and optical generation in photorefractive strontium niobate crystals," *Sov. Tech. Phys. Lett.*, **12**, 608, 1987.

41. M. Saffman, D. Montgomery, A. A. Zozulya, K. Kuroda and D. Z. Anderson, "Transverse instability of counterpropagating waves in photorefractive media," *Phys. Rev.*, **A48**, 3209, 1993.

42. Z. Chen and N. B. Abraham, "Pattern dynamics in a bidirectional photorefractive ring resonator," *Appl. Phys.*, B S183, 1995.

43. J. Malos, M. Vaupel, K. Staliunas and C. O. Weiss, "Dynamical structures of a photorefractive oscillator," *Phys. Rev.*, **A53**, 3559, 1996.

44. B. Sturman and A. Chernykh, "Mechanism of transverse instability of counterpropagation in photorefractive media," *J. Opt. Soc. Amer.*, **B12**, 1384, 1995.

45. M. Saffman, A. A. Zozulya and D. Z. Anderson, "Transverse instability of energy-exchanging counterpropagating waves in photorefractive media," *J. Opt. Soc. Amer.*, **B11**, 1409, 1994.

46. P. P. Banerjee, J. O. Dimmock and N. V. Kukhtarev, "Self-organization in photorefractive crystals in the presence of transmission and reflection gratings," *SPIE Proc.*, **2849**, 79, 1996.

47. P. P. Banerjee, J. O. Dimmock, F. L. Madarasz and N. V. Kukhtarev, "Steady state analysis of self-organization of light into a scattering ring due to induced reflection gratings in photorefractive materials," *J. Opt. Soc. Amer. B* (submitted for publication).

48. J. O. Dimmock, P. P. Banerjee, and N. V. Kukhtarev, "Analysis of the self-organization of light due to induced reflection gratings in potassium niobate," *Proceedings of the SPIE, Photorefractive Fiber and Crystal Devices: Materials, Optical Properties and Applications III,* **3137**, 75, 1997.

49. P. Yeh, *Introduction to Photorefractive Nonlinear Optics*, Wiley, New York 1993.

50. N. V. Kukhtarev, P. Buchhave, S. F. Lyuksyutov, T. Kukhtareva, K. Sayano, F. Zhao and P. P. Banerjee, "Self-enhancement of dynamic gratings in photogalvanic crystals," *Phys. Rev. A,* **58**, 4051, 1998.

51. P. P. Banerjee, J. O. Dimmock, F. L. Madarasz and N. V. Kukhtarev, "Effect of the phase of the coupling constant on the self-organization of light in potassium niobate," *SPIE Proc. Annual Meeting,* San Diego, CA, 1998.

52. J. O. Dimmock, "Symmetry considerations in the formation and rotation of hexagonal scattering patterns in photorefractive $KNbO_3$," *SPIE Conference on Photorefractive Fiber and Crystal Devices: Materials, Optical Properties and Applications II,* Denver, **2849**, 1996.

53. O. Sandfuchs, J. Leonardy, F. Kaiser and M. R. Belic, "Transverse instabilities in photorefractive counterpropagating two-wave mixing," *Opt. Lett.*, **22**, 498, 1997.

54. W. J. Firth, "Spatial instabilities in a Kerr medium with a single feedback mirror," *J. Mod. Opt.*, **37**, 151, 1990.

55. G. D'Alessandro and W. J. Firth, "Hexagonal spatial patterns for a Kerr slice with a feedback mirror," *Phys. Rev.*, **A46**, 537–548, 1992.

56. N. B. Abraham and W. J. Firth, "Overview of transverse effects in nonlinear optical systems," *J. Opt. Soc. Amer.*, **B7**, 951, 1990.

57. S. Mallick, B. Imbert, H. Ducollet, J. P. Herriau and J. P. Huignard, *J. Appl. Phys.*, **63**, 5660, 1998.

58. D. Jones and L. Solymar, *Opt. Lett.*, **14**, 743, 1989.

59. B. I. Sturman, A. Bledowski, J. Otten and K. H. Ringhofer, *J. Opt. Soc. Amer.*, **B9**, 672, 1992.

60. N. Kukhtarev, T. Kukhtareva, A. Knyaz'kov and H. J. Caulfield, *Optik*, **97**, 7, 1994.